Three-dimensional electrons and two-dimensional electric subbands in the transport properties of tin-doped *n*-type indium selenide: Polar and homopolar phonon scattering

A. Segura, B. Marí, and J. Martinez-Pastor
Departament de Física Aplicada, Facultat de Física, Universitat de València, 46100 Burjassot (Valencia), Spain

A. Chevy
Laboratoire de Physique des Milieux Condensés, 4 place Jussieu, Tour 13, 75005 Paris, France
(Received 7 August 1989; revised manuscript received 24 October 1990)

Electron-scattering mechanisms in *n*-type indium selenide doped with different amounts of tin are studied by means of the Hall effect (30–300 K) and photo-Hall effect (300 K). The electron mobility at room temperature is found to increase with the free-electron concentration in samples with low tin content. The same behavior is observed when the electron concentration increases due to thermal annealing or photogeneration. That is explained through the presence of two kinds of free electrons contributing to the charge transport along the layers: high-mobility three-dimensional (3D) electrons in the conduction band, and low-mobility two-dimensional electrons in the electric subbands. These 2D subbands are proposed to exist in InSe due to size-quantization effects in thin layers located between two stacking faults. In these regions electron states become higher than conduction-band states. Electrons are transferred outside these regions and are confined in 2D subbands by the resulting electric field. In regard to the electron-scattering mechanisms, it is shown that LO polar phonons play an important role in the scattering of 3D electrons, whose mobility has been calculated by an iteration method. From a comparison with experimental results, we show that the coupling constant for the 3D electron-phonon deformation-potential interaction has been overestimated in previous calculations The relaxation time for the scattering of 2D electrons by homopolar phonons is determined by using a variational wave function, and the calculated 2D mobility decreases when the localization of the 2D subbands along the *c* axis increases.

I. INTRODUCTION

The transport properties of indium selenide (InSe) along the layers have been widely investigated in the past twenty years.[1–10] At high temperature ($T > 100$ K) the electron Hall mobility μ_{eH} can be expressed in a given temperature range in the form $\mu_{eH} \propto T^{-\gamma}$, where the exponent γ varies between 1.45 and 2. Experimental results have been analyzed in the framework of the Schmid and Fivaz model for homopolar phonon scattering.[11–13] According to this model, the exponent γ depends on the energy $\hbar\omega_{\rm ph}$ of the phonons that scatter the electrons, and the dimensionality of the electron gas.

Table I summarizes the main results found in the literature about the electron scattering in InSe. The first thing to point out is the fact that only in Refs. 5, 9, and 10 ionized impurity scattering is taken into account in a quantitative interpretation of the temperature dependence of electron mobility. However, most of the reported experimental results strongly suggest the presence of such a scattering mechanism. The values of the phonon energy and the electron-phonon coupling constant, obtained with a model that only includes scattering by lattice vibrations, are hardly significant.

It is also evident that there is no agreement upon the dimensionality of charge transport in InSe among the different authors. While the three-dimensional (3D) character of InSe is theoretically (band-structure calculations[14]) and experimentally (cyclotron resonance measurements[15]) well established, some authors interpret their data with a 2D model. The observed 2D behavior has been related to the existence of 2D electric subbands in electron accumulation layers created by planar aggregates of donor impurities bound to stacking faults.[15–19] The relaxation time for homopolar optical-phonon scattering in the 2D case was deduced by Fivaz and Mooser[11] under the assumptions of a 2D density of states and translational symmetry along the *c* axis. Then it cannot be applied to electrons in an electric subband because the second condition is not fulfilled, its localization along the *c* axis being strongly dependent on the shape of the potential near to the planar defect.

Table I reflects the fact that all the authors have only invoked scattering by the homopolar optical phonon in order to interpret the temperature dependence of electron mobility in InSe. Schmid and Fivaz[11–13] have emphasized that this peculiarity of layered semiconductors is related to the low site symmetry in these materials, that leads to very high electron-phonon deformation potentials. In fact, the existence of electron-deformation-potential interaction has been recently confirmed by Howell *et al.*[20] through cyclotron-resonance (CR) experiments in the InSe 2D electron gas at 1.5 K and with magnetic fields up to 25 T. Nevertheless, they estimate a very low coupling constant ($g^2 \approx 0.0015$) of 2D electrons to the 14.3-meV A_1' homopolar phonon, in contrast with

TABLE I. (1) Literature results on electron scattering in InSe: (2) temperature range, (3) electron mobility at 300 K, (4) maximum electron mobility, (5) temperature at which it occurs, (6) slope at 300 K of the double logarithmic plot mobility vs temperature, (7) slope at 100 K, (8) energy of the homopolar optic-phonon coupled to electrons, (9) electron-phonon coupling constant, (10) dimensionality of the electron gas.

1	2	3	4	5	6	7	8	9	10
Reference	Temperature range (K)	$\mu_{300\ K}$ ($cm^2/V\,s$)	μ_{max} ($cm^2/V\,s$)	T_{max} (K)	$\gamma_{300\ K}$	$\gamma_{100\ K}$	$\hbar\omega_{ph}$ (meV)	g^2	D
1	100–600	650	890	350	−1.50[a]	−1.50	29.7	0.025	2
2,3	4–300	900	10 000	60	1.60	1.60			
4	140–300	400	900	200	2.00	−1.50[b]	22.0	0.250	3
5	4–500	980	40 000	30	1.70	2.20	14.3	0.054	3
6	100–300	700	3 100[c]		1.55	1.55	14.3	0.069	2
8	4–300	600	16 000	40	1.44	2.10			
9	85–300	850	8 500		1.70	1.90	14.3	0.063	3
10	80–300	990	11 890		1.43	2.50	14.3	0.015	2

[a]In this reference the dependence $\mu \propto T^{-2}$ occurs for $T > 400$ K.
[b]This value of γ corresponds to the interval 140–200 K.
[c]This value corresponds to 100 K. In the studied temperature range $\mu(T)$ does not exhibit a maximum.

values of Table I. We believe that their estimation is not well founded because it is based on the self-energy equation given by Schmid[12] for the 3D case. Even the use of the Fivaz-Schmid equation for the 2D case[13] would be inadequate as well due to the lack of translational symmetry. Indeed, if g^2 is estimated from the cyclotron mass discontinuity occurring when the Landau level energy crosses the A_1' phonon energy (Fig. 1 in Ref. 20) by using the effective-mass renormalization equation given by Fivaz and Schmid,[13] the value of g^2 would be comprised between 0.015 and 0.03, which is half the lower value in Table I and would lead to electron mobilities higher than 2000 $cm^2/V\,s$ at room temperature. The results of Howell *et al.*[20] also show that the coupling of 2D electrons in InSe to LO polar phonons is very strong.

A reexamination of the electron-scattering mechanisms in InSe is then necessary, especially in those which concern the role of LO polar phonon scattering in both the 3D and 2D cases, which have been neglected up to now. A more realistic approach to the problem requires, on the one hand, systematic measurements in InSe samples with different free-electron and impurity concentrations, in order to elucidate the influence of impurity scattering. That can be achieved by doping with tin, which turns out to be a quite reproducible way of controlling the electron concentration in InSe.[21,22] On the other hand, a model of the electronic levels in the 2D defects is needed if one intends to determine how electrons in the 2D subbands contribute to charge transport in InSe.

In this paper, we report Hall-effect (HE) measurements in the n-type InSe samples with different tin contents. Experimental results are presented in Sec. III. Section IV is devoted to the discussion and interpretation of experimental results on the basis of a model in which both 2D and 3D electrons are taken into account in the whole temperature range and 2D subbands are related to size-quantization effects in thin layers between two stacking faults. Polar phonon scattering of 3D electrons is shown to be relevant at room temperature. The introduction of such scattering mechanism involves the use of the iteration method in the calculation of electron mobilities. As a result, the coupling constant of 3D electrons to homopolar phonons is shown to have been overestimated in previous calculations.

In this paper we will limit ourselves to the problem of phonon scattering, and a model for homopolar phonon scattering in 2D subbands is proposed in Sec. IV. Impurity scattering will be discussed in a future paper where HE measurements at liquid-helium temperature will be reported.

II. EXPERIMENT

InSe monocrystals have been grown by the Bridgman method from a nonstoichiometric melt $In_{1.05}Se_{0.95}$. The tin is introduced in the preparation of the polycrystalline melt as SnSe.[23] The percents of tin used are 0.01, 0.03, 0.1, 1, 3, and 10. It has been shown[24] that only a small part of the tin remains in the InSe crystal, the rest being rejected to the end of the ingot.

Samples were cleaved from the ingots with a razor blade and cut into parallelepipeds 10–20 μm thick and about 3×5 mm^2 in size. Evaporated In contacts were made in the classical configuration for such sample shape. The resistivity and HE measurements as a function of temperature were made in a closed-cycle Leybold-Heraeus cryogenic system. The magnetic field intensity was 0.6 T. The photo-HE measurements were carried out by illuminating the sample with infrared light emitted by a GaAs electroluminescent diode. Several samples with low tin content were also studied after annealing them in vacuum at 300 °C for 1 h.

III. RESULTS

Figures 1 and 2 show the electron Hall mobility μ_{eH} versus absolute temperature for several samples from each ingot. Table II gives the mean values of μ_{eH} at 300 and 30 K, the maximum value of μ_{eH}, the temperature at which it occurs, the mean electron concentration at 300

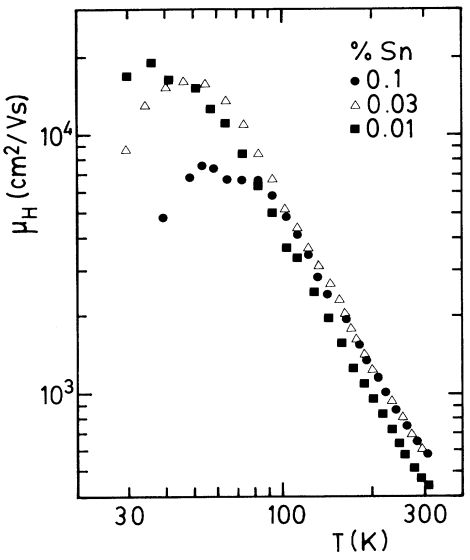

FIG. 1. Hall mobility vs absolute temperature for low-tin-content samples.

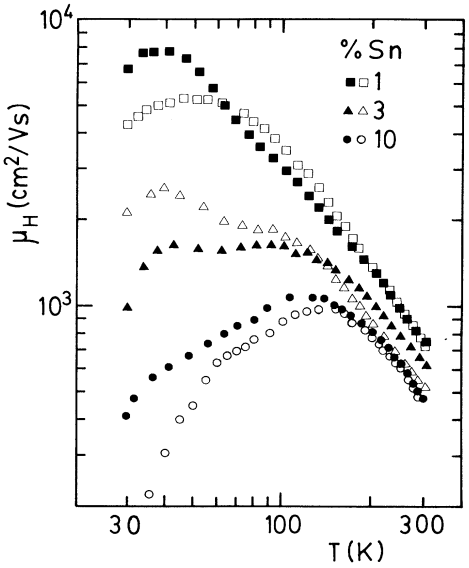

FIG. 2. Hall mobility vs absolute temperature for high-tin-content samples.

K and the γ exponent at 300 and 100 K. The electron concentration has been calculated from the Hall coefficient with the assumption that the Hall factor is 1, which has been widely discussed in Refs. 5 and 11. Figure 3 shows the Hall mobility at 300 K as a function of the electron concentration in the different samples.

The evolution of the temperature dependence of electron mobility with tin content corresponds, in general, to the expected behavior. Nevertheless, an anomaly is observed at room temperature in the samples with the lowest tin contents (0.01%, 0.03%, 0.1%, and 1%): the electron mobility turns out to increase with the electron concentration (Fig. 3). Two more experiments confirm that this behavior is a property of these InSe samples independent of the way in which the free-electron concentration increases.

A. Photo-HE measurements

Table III gives the results of HE and photo-HE measurements in three samples from the 0.01% tin-doped ingot. The photoenhancement of electron mobility is apparent. This effect is stronger for samples with lower electron mobility in the dark (see column 5 in Table III).

B. HE measurements in thermally annealed samples

It has been shown[5] that the room-temperature electron concentration in n-type InSe samples increases from 10^{15} cm^{-3} to more than 10^{16} cm^{-3} after thermal annealing at temperatures higher than 300 °C, and then relaxes to the previous value in a slow process than can last several days. Table IV shows the results of such experiment for several samples from the 0.01% tin-doped ingot. The electron Hall mobility increases by nearly 80% when the electron concentration varies from 10^{15} to 2.10^{16} cm^{-3}. Figure 4 shows the temperature dependence of Hall mobility for one sample of the 0.01 Sn-doped ingot before and immediately after annealing. The increase of Hall mobility in the high-temperature range after annealing is clearly illustrated.

A word should be said about the behavior of the ex-

TABLE II. Summary of the transport properties of tin-doped InSe: (1) tin content, (2) room-temperature electron mobility, (3) electron mobility at 30 K, (4) maximum electron mobility, (5) temperature at which it occurs, (6) slope at 300 K of the double logarithmic plot $\mu(T)$, (7) slope at 100 K, (8) electron concentration at room temperature.

1 Tin content (%)	2 $\mu_{300\ K}$ (cm^2/V s)	3 $\mu_{30\ K}$ (cm^2/V s)	4 μ_{max} (cm^2/V s)	5 T_{max} (K)	6 $\gamma_{300\ K}$	7 $\gamma_{100\ K}$	8 $n_{300\ K}$ (10^{15} cm^{-3})
0.01	550	20 000	21 400	40	1.70	2.20	1.5
0.03	700	8 000	15 500	50	1.75	2.15	1.9
0.1	720	4 000	7 000	60	1.70	1.90	4.1
1	860	2 500	5 200	80	1.60	1.10	42.0
3	700	1 500	1 740	90	1.25	0.65	57.0
10	600	400	1 100	130	1.15	−0.60	110.0

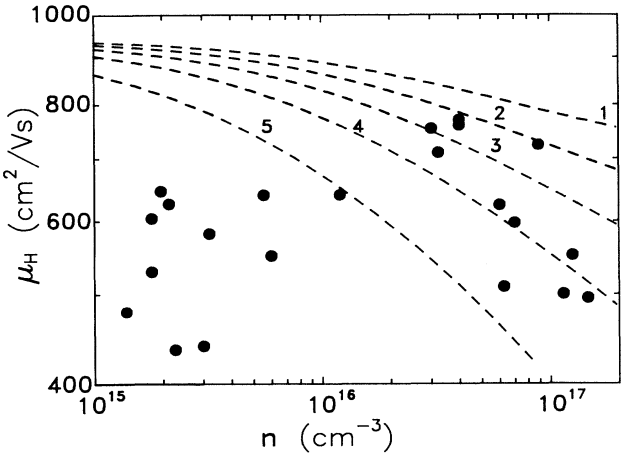

FIG. 3. Room-temperature electron Hall mobility vs electron concentration in tin-doped InSe (experimental points) and calculated electron mobility at room temperature vs electron concentration (dotted lines) for several values of the compensation ratio: (1) no compensation, (2) 20%, (3) 40%, (4) 60%, and (5) 80%.

ponent γ. At room temperature γ has nearly the same value in the low tin content samples, while in the high tin content ones it depends on the electron concentration. Around 100 K, γ is also strongly dependent on the tin content. This is also the case for the maximum mobility and the temperature at which it occurs.

IV. DISCUSSION

A. Scattering mechanisms of 3D electrons in InSe

Results of HE measurements on InSe samples with the highest electron mobility (10^3 and 4.10^4 cm^2/V s at 300 and 30 K, respectively) were published in Ref. 5. It was shown that the temperature dependence of electron mobility in the range from 40 to 300 K can be quantitatively accounted for by a 3D model, in which three scattering mechanisms were considered: (i) homopolar optical phonons, through the Schmid-Fivaz 3D relaxation time;[12,13] (ii) ionized impurity scattering through the Brooks-Herring relaxation time;[25] and (iii) neutral impurity scattering through the Erginsoy relaxation time.[26]

The large dispersion of values of homopolar optical-phonon coupling constant g^2 and a recent paper by Howell *et al.*,[20] where g^2 could be as low as 0.0015, make it necessary to consider (i) if there is another contribution to the mobility, coming from a scattering mechanism that has not been taken into account up to now; (ii) if the dimensionality of that model is correct. Cyclotron resonance results,[15,17] as well as the temperature dependence of the electron concentration,[21] suggested that free electrons in those InSe samples have 3D character and that only below 20 K they behave strictly two dimensionally. Then the study of the mobility in the 40–300 K temperature range must be done with a 3D model.

The possible scattering mechanism that have not been considered are LA phonons and LO polar phonons. A first approximation of the deformation potential for LA phonons comes from the volume compressibility[27] and the pressure coefficient of the gap,[28–30] which yields $E_{ac}=1.4$ eV. Another estimation, based on the GaSe deformation potential calculated by Schlüter[31] for changes in the Ga—Se bond yields $E_{ac}=3.2$ eV. Even with the highest value of E_{ac} and taking the elastic modulus at InSe $C_{11}=1.18\times10^{11}$ Pa,[32] the Bardeen-Shockley model[33] for acoustic-phonon scattering leads to an electron mobility of the order of 9×10^4 cm^2/V s at 300 K, two orders of magnitude higher than the actual values, which means that the effect of acoustic phonons can be neglected.

In the case of LO polar phonons we have calculated the Fröhlich constant[34] in InSe taking the CR electron effective mass,[15] the dielectric constants, and LO polar phonon frequencies from Refs. 35–37, which yields, respectively, 0.26, 0.31, and 0.31 for $\alpha_\perp$, and 0.06, 0.075, and 0.073 for $\alpha_\parallel$. As the electron-scattering rates for LO polar phonons are obtained through an integration over all the possible directions of the phonon moment, we have taken an angular average of the Fröhlich constant over the whole solid angle. Assuming the main angular dependence of the Fröhlich constant arising from the angular variation of the dielectric constant,[38] we obtain $\bar{\alpha}=0.144$ (for $\alpha_\perp=0.3$ and $\alpha_\parallel=0.07$). With that value of $\bar{\alpha}$ and taking $\hbar\omega_{LO}=27.3$ meV,[35–37] we have calculated the LO polar phonon limited electron mobility through an interaction method.[39,40] Curve 2 in Fig. 5 is the result of that calculation. If we compare it with the experimental results in the highest mobility samples[5] reproduced as open squares in Fig. 5, it is clear that LO polar phonons are important in determining the electron mobility in

TABLE III. Photo-Hall-effect results in 0.01% Sn-doped InSe. Resistivity (column 2), electron concentration (column 3), and mobility (column 4) in the dark (D) and under illumination (I); (5) ratio of the relative increase of the Hall mobility to the relative increase of electron concentration.

1	2		3		4		5
	ρ		n		μ		
Sample	(Ω cm)		(10^{15} cm^{-3})		(cm^2/V s)		$\frac{\Delta\mu/\mu_D}{\Delta n/n_D}$
	D	I	D	I	D	I	
1	9.00	6.18	1.48	1.73	470	584	1.43
2	8.99	6.34	1.08	1.39	645	710	0.38
3	9.30	7.50	1.27	1.45	529	573	0.58

TABLE IV. HE results in annealed samples. Resistivity (column 2), electron concentration (column 3), and mobility (column 4) of two samples before (B) and after (A) annealing.

1	2		3		4	
Sample	ρ (Ω cm)		n (10^{15} cm^{-3})		μ (cm^2/V s)	
	B	A	B	A	B	A
1	12.4	0.42	1.23	21.6	408	682
2	9.3	0.27	1.27	26.0	529	895

InSe. It is also clear that the mobility, calculated considering only polar phonon scattering, cannot explain the temperature dependence in the high-temperature range. At high temperature the LO polar phonon mobility tends to the well-known dependence $\mu_{LO} \propto T^{-1/2}$, whereas the experimental mobility decreases with a higher slope ($\mu \propto T^{-1.7}$). We must then introduce the homopolar phonon scattering, along with the other considered in Ref. 5 (ionized and neutral impurity scattering). For those mechanisms a relaxation time can be used and they are introduced in the elastic term of the scattering rates. In this way, we have fitted the experimental results in a nonintentionally doped sample, characterized by high mobility values and low-impurity concentration. Then the fitting procedure only involves the coupling constant of electrons to the 14.3-meV A_1' homopolar phonon g^2 as the main adjustable parameter, yielding a value of $g^2=0.028$. Therefore LO polar scattering results in a reduction of g^2 by a factor of 2 with respect to the lowest value in Table I. That value is higher than the estimation of Howell *et al.*[20] We believe that their estimation is not well founded as their results refer to 2D electrons at 1.5 K in an accumulation layer and they use equations for 3D electrons in their discussion. We will see later that

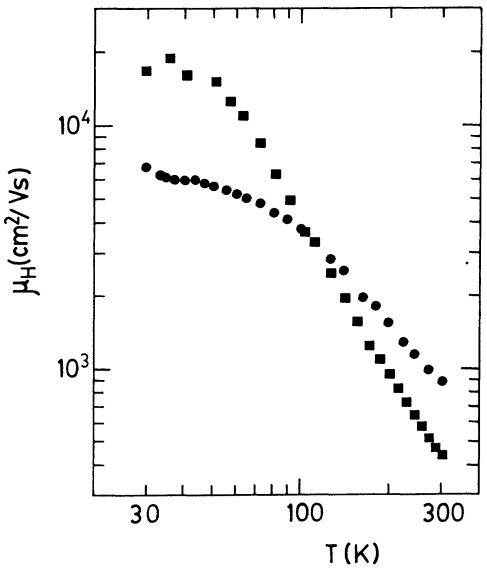

FIG. 4. Electron Hall mobility vs absolute temperature of a sample from the 0.01% Sn-doped ingot before (■) and after annealing (●).

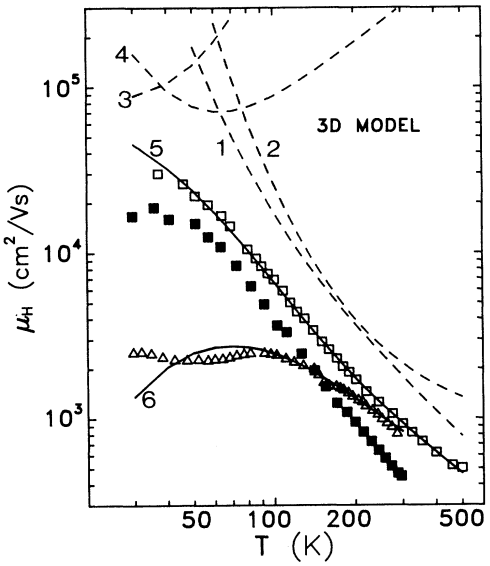

FIG. 5. Electron Hall mobility vs absolute temperature of three samples from the 0.01% Sn-doped ingot (■), 3% doped ingot (△), and high-mobility ingot from Ref. 5 (□). Curve 5 is the calculated mobility that fits the highest mobility sample. The dotted lines represent the different contributions to that curve: (1) homopolar and (2) polar optical-phonon scattering, (3) neutral and (4) ionized impurity scattering. Curve 6 is the calculated mobility curve fitting the 3% Sn sample.

the effective coupling constant of 2D electrons depends on the electron areal concentration and can be higher or lower than the 3D one.

Once the coupling constant has been obtained from the fitting with undoped samples, the mobility in high-impurity concentration samples can be explained, as shown in Fig. 5 (curve 6). We can consider the results for high-mobility samples in Ref. 5 and results for high-tin-concentration samples reported here as representative of the transport properties of 3D electrons in InSe, as they can be interpreted through the 3D model.

B. Failure of the 3D model

The mobility curves of the low-tin-content samples cannot be explained with the 3D model. The measured electron concentration in these samples is practically the same as that of high-mobility samples and the 3D model would lead to the same mobility (Fig. 5).

Figure 3 show the mobility at room temperature in samples with different impurity concentration. When the electron and impurity concentration increase, the effect of impurity scattering always makes the calculated electron mobility decrease. The dotted lines in Fig. 3 correspond to the calculated electron mobility at room temperature for different values of the compensation ratio N_D/N_A (see caption of Fig. 3). On the other hand, the values of the electron mobility in samples with $n > 4.10^{16}$ cm^{-3} lie in the range of the calculated ones, if compensation ratios between 20% and 80% are considered. The lowest one is obtained from a single-donor–single-

acceptor fit to the $n(T)$ results.[22] The highest one (80%) is yielded by a quantum-mechanical interpretation of free carrier absorption in these samples.[41]

C. Model with two kinds of electrons

The discussion of Sec. IV A has shown that electrons in the low-tin-content material have different transport properties than electrons in high-tin-content samples and in high-electron-mobility samples (undoped). The lower mobility cannot be attributed to any kind of impurity scattering since its temperature dependence clearly reveals that a lattice scattering mechanism is dominant (Fig. 1).

The fact that the increase of electron concentration in a sample makes electron mobility approach 3D values suggests that electrons in low-tin-content InSe can have 2D character and lower mobility. This idea is also supported by photo-HE results: photogenerated electrons are uniformly created through the sample by band-to-band transitions and have clearly 3D character. Their higher mobility would explain the photoenhancement in the Hall mobility.

The existence in InSe of strictly 2D electrons that do not take part in the charge transport across the layers and predominate for low-tin-content samples is also coherent with the observed high-anisotropy ratio of resistivity and its dependence on temperature and tin content.[42]

All these considerations are brought forward as indirect clues suggesting the presence in InSe of two kinds of electrons. In fact, CR measurements[15,17] have clearly shown the coexistence in InSe of 2D and 3D electrons through the temperature range from 15 to 95 K, the resonance lines become too broad to be observed, but there is no reason to conclude that one of these types of electrons disappears.

Let us assume that the material is homogeneous along the layers and that the only inhomogeneity across the layer is due to the presence of the planar defects where 2D electrons are localized. Then the electron concentration can be expressed as

$$n(x)=n_3+\sum_i n_S^i \delta(x-x_i) , \tag{1}$$

where x is the coordinate perpendicular to the layers, n_3 is the concentration of 3D electrons, and n_s^i is the density of 2D electron per unit area in the planar defect, located at x_i. In a HE experiment with current flowing parallel to the layers, both kinds of electrons take part in the charge transport. The Hall coefficient, conductivity, and Hall mobility can be easily deduced from Eq. (1):[43]

$$R_H=\frac{1}{q}\frac{n_2\mu_2^2+n_3\mu_3^2}{(n_2\mu_2+n_3\mu_3)^2} , \tag{2}$$

$$\sigma=q(n_2\mu_2+n_3\mu_3) , \tag{3}$$

$$\mu_H=\frac{n_2\mu_2^2+n_3\mu_3^2}{n_2\mu_2+n_3\mu_3} , \tag{4}$$

where $n_2=\sum_i n_s^i/d$, d is the sample thickness, and μ_3 and μ_2 are the mobilities of each type of electrons.

Equation (4) gives a qualitative interpretation of the experimental results provided one assumes $\mu_3\approx 2\mu_2$. In low-tin-content samples 2D electrons are dominant and $\mu_H\approx\mu_2$. When the tin content increases n_3 also increases, and then μ_H varies from μ_2 to μ_3. For high-tin-content samples $n_3 \gg n_2$ and $\mu_H\approx\mu_3$ and the 3D model described in Sec. IV A can be used. A quantitative interpretation of the results requires a model of the planar defect and the related 2D subbands, which will allow us to calculate the 2D electron mobility.

D. Models for the 2D subbands in InSe

Since it was proposed by Portal and co-workers,[15,19] the 2D subbands in InSe have been considered as mainly arising from the binding of electrons to planar sheets of ionized shallow donors adsorbed to stacking faults. These authors have also suggested that the stacking fault could correspond to the boundary between two different polytypes of InSe, resulting in a band-gap discontinuity. The physical consequences of each of these models have not been discussed so far and in fact, only a band scheme of the first one has appeared in the literature[15] and is reproduced in Fig. 6(a). Recently, Howell *et al.*[20] have proposed that the 2D subbands in InSe are analogous to the δ-doped structures.[44–48] The δ-doping model does not work in InSe for several reasons.

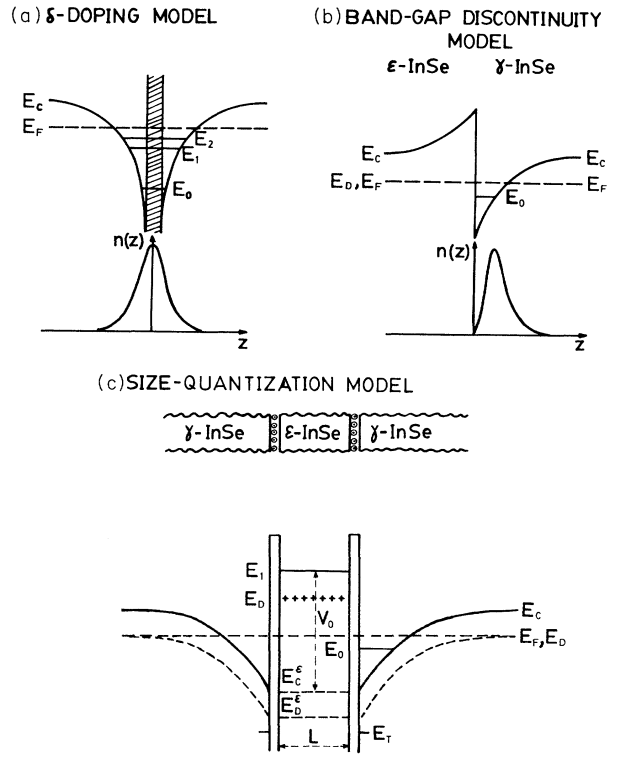

FIG. 6. Band schemes for the 2D subbands in InSe: (a) δ-doping model, (b) band-gap discontinuity model, and (c) size-quantization model. In (a) and (b) the electron density in the lowest subband is also shown. In the model of (c) the electron density would be the same as (b).

(i) δ-doping subbands are in fact 2D bands of impurities. This involves the existence of a critical impurity concentration below which extended states cannot exist, and a metal-insulator transition occurs. This is observed in silicon δ-doped GaAs for silicon areal concentration below 2×10^{11} cm^{-2},[45] which corresponds to $0.2(a_0^*)^{-2}$,[49] where a_0^* is the effective Bohr radius of the hydrogenic impurity. Using the same criterion in InSe, where $a_0^*\approx38$ Å,[15] the impurity and electron concentration in a 2D subband of that nature must be higher than 1.4×10^{12} cm^{-2}. The electron concentration at 4 K ranges from 10^{13} cm^{-3} in the samples' growth by the traveling-heat method[9] (THM) to 5×10^{14} cm^{-3} in Bridgmann samples.[5] This leads to a mean distance between planar defects along the c axis ranging from 30 μm to 2 mm.

A large series of samples with thicknesses ranging from 5 to 50 μm was measured in Ref. 5 and the degenerate behavior below 20 K was always observed. Then the mean distance between planar defects responsible for the 2D subbands must be much lower than 30 μm. A mean distance of 2–5 μm seems to be more reasonable, which would correspond to electron areal concentrations always lower than 3×10^{11} cm^{-2}. This value is in agreement with the values reported by Howell *et al.*,[20] Belen'kii *et al.*,[50] and Brandt *et al.*[51] (approximately equal to 10^{11} cm^{-2}). The critical concentration would be one order of magnitude higher and that clearly contradicts the δ-doping model.

(ii) The electron wave function in the lowest subband of a δ-doped structure has its maximum at the impurity plane,[45,47,48] as shown in Fig. 6(a). Electrons move very close to ionized impurities and have very low mobility. This is the case for silicon δ-doped GaAs structures, in which electron mobilities at 4 K are of the order of 1200 $cm^2/V\,s$ for an impurity concentration of 7.5×10^{11} cm^{-2}.[47] Electron mobilities in InSe are always lower than in GaAs, with similar impurity concentrations, by a factor of 6–7 (due to higher electron effective mass and lower dielectric constant in InSe). One should expect an electron mobility lower than 200 $cm^2/V\,s$ but values as high as 1.5×10^4 $cm^2/V\,s$ have been measured at 4.2 K.[5] Only 2D electrons are present in InSe (Refs. 5, 15, and 16) at this temperature, and consequently, 2D electrons must be spatially separated from ionized impurities.

(iii) Kress-Rogers *et al.*[19] have determined a maximum of 10^{10} cm^{-2} ionized impurities in InSe subbands from an analysis of the magnetic-field dependence of the cyclotron resonance linewidth (CRLW), which is one order of magnitude lower than the electron concentration. In a δ-doping model ionized impurity and electron concentrations must be identical. Moreover, the CRLW turns out to be controlled by neutral impurity scattering. This means that most impurities adsorbed to the defect plane are neutral, and then the related energy levels must be deeper than the 2D subbands.

(iv) In regard to the potential seen by 3D electrons along the c axis, the activated temperature dependence of the resistivity anisotropy suggests the presence of potential barriers. Instead of it, the δ-doping model only predicts accumulation layers and then 3D electrons only see potential wells when moving along the c axis.

It seems reasonable to conclude that a δ-doping model is unable to explain the properties of 2D electrons in InSe. If a new model is proposed, it must necessarily include a spatial separation between ionized impurities and 2D electrons. In this direction, a model based in the band-gap discontinuity between the ϵ and γ polytypes of InSe could overcome the last objections. The presence of small regions of the ϵ polytype in Bridgmann samples has been proved by electron diffraction[52] and Raman scattering.[53,54] Figure 6(b) shows the band scheme of this model. The band gap of the ϵ polytype has been assumed to be above the conduction band in the γ polytype. Shoubnikov–de Haas (SdH) measurements[18] indicate that the bottom of the 2D subbands is about 10 meV below the Fermi level and about 30 meV below the conduction band. A band-gap discontinuity larger than 40 meV would be needed in order to obtain such a subband configuration. In the case of GaSe, where β, ϵ, δ, and γ polytypes have been studied, the higher difference (about 25 meV) occurs between the β polytypes and the other ones.[55] Between ϵ and γ polytypes the difference is not larger than 5 meV. The similarity of both types of stacking excludes larger differences and band-structure calculations are coherent with that result.[56] In InSe, the differences between the ϵ and γ polytypes are not expected to be larger than in GaSe. On the other hand, Guatenko *et al.*[57] have reported photoluminescence experiments in γ-ϵ samples and they attribute the higher energy peaks to free excitons in ϵ and γ polytypes, the former being 2–3 meV higher than the latter. We can conclude that such little band-gap discontinuities cannot be the origin of the 2D subbands in InSe.

Stacking faults, whose presence and effects on transport and optical properties have been widely investigated,[13,58–60] provide a basis for another model. It has been proved that stacking faults can create barriers of some tens of meV.[58] Stacking faults are associated with the change of the stacking sequence, and then can correspond to the interface between the polytypes γ and ϵ in our samples. Then thin regions of the ϵ polytype would be limited by stacking faults barriers. In those regions all the electron levels would be raised by quantum confinement effects. Figure 6(c) shows a band scheme for that model. For a 2D subband to be created, the shallow donor levels in the thin ϵ region must be raised by at least 20 meV, becoming higher than the conduction band in the γ region. Electrons from those donors would be transferred to the conduction band of the adjacent γ region leaving an uncompensated positive charge, which gives rise to an attractive electric field at the interface. This electric field and the presence of the stacking faults barriers create a 2D subband with a spatial separation between donors and electrons. This model turns out to be very similar to some structures in which a δ-doped GaAs layer is separated from the bulk material by two thin $Ga_xAl_{1-x}As$ layers, keeping electrons apart from impurities and avoiding the low electron mobility of normal δ-doping subbands.[44]

In the simplest square-well approximation the conduction-band states become a series of 2D subbands

given by

$$E_n(\mathbf{k}_{xy})=\frac{\hbar^2\pi^2 n^2}{2m_{\parallel}^* L^2}+\frac{\hbar^2 k_{xy}^2}{2m_{\perp}^*} , \tag{5}$$

where $m_{\parallel}^*=0.08m_0$ and $m_{\perp}^*=0.14m_0$ (Ref. 15) are the electron effective masses in InSe parallel and perpendicular to the c axis (z axis), respectively, and L is the width of the ϵ region between two stacking fault barriers. The bottom of the first subband is then at an energy $V_0=\hbar^2\pi^2/2m_{\parallel}^* L^2$, higher than the conduction band. If we neglect the normal band-gap discontinuity between the ϵ and γ polytype, we can identify V_0 with the band-gap offset, which results higher than 40 meV if L is about 10 nm. If we assume that shallow levels in the ϵ region also raise the same quantity V_0, all electrons from donors in the ϵ layer will go to the γ region and the ϵ layer becomes fully depleted. If we call N_D^{ϵ} the shallow donor concentration in that layer, and assume a homogeneous distribution, the 2D electron concentration at both sides of the ϵ region would be $n_S=N_D^{\epsilon}L/2$.

If only the lowest subband is occupied, the condition to have a fully depleted ϵ layer follows straightforwardly from the band scheme of Fig. 6(c):

$$V_0>E_0+(E_F-E_0)+E_D+E_B . \tag{6}$$

E_0 is the bottom of the lowest subband, E_D is the ionization energy of shallow donors in the γ region, at whose energy the Fermi level is assumed to be locked at low temperature, and E_B/q is the built-in potential created by the space-charge in the ϵ region.

Regardless of the origin of the discontinuity (ϵ-γ band-gap offset or size-quantization effects), both models are quite similar, and the 2D subband wave function will be in both cases determined by the electric field in the interface and the presence of the potential barrier. Then the localization of electrons in the lowest subband is described by the usual variational function[61]

$$\chi_0(z)=\left[\frac{b_0^3}{2}\right]^{1/2} z e^{-b_0 z/2} . \tag{7}$$

If the compensation in the γ region is very weak, the variational Hartree calculation in which the total energy is minimized leads to[61]

$$E_0=\frac{5}{8}\frac{\hbar^2 b_0^2}{m_{\parallel}^*} ,$$
$$b_0=\left[\frac{33q^2 m_{\parallel}^* n_S}{8\epsilon_{\parallel}\hbar^2}\right]^{1/3} . \tag{8}$$

The use of a variational wave function is a rough approximation. The potential barriers at the stacking faults are thin and not very high and a more realistic model should allow for a penetration of the electron wave function in the ϵ layer. That would modify the potential energy and then E_0 and the relationship between E_0, b_0, and n_S. From the point of view of transport properties, when dealing with impurity scattering, Eq. (7) will be very inadequate as it will underestimate the effect of such scattering mechanism. If we limit ourselves to the problem of phonon scattering, Eq. (7) can give a first approximation that should not be dramatically modified when an exponential tail penetrating in the ϵ region is introduced in the wave function.

The E_F-E_0 energy is obtained from the density of states in the 2D gas:

$$E_F-E_0=\frac{\hbar^2\pi}{m_{\perp}^*}n_S \tag{9}$$

and the built-in potential is given by the usual expression

$$V_B=\frac{qn_S^2}{2\epsilon_{\parallel}N_D^{\epsilon}}=\frac{qn_S L}{4\epsilon_{\parallel}} . \tag{10}$$

Then Eq. (6) can be rewritten as

$$\frac{\hbar^2\pi^2}{2m_{\parallel}^* L^2}>\frac{5}{8}\frac{\hbar^2}{m_{\parallel}^*}\left[\frac{33q^2 m_{\parallel}^* n_S}{8\epsilon_{\parallel}\hbar^2}\right]^{2/3}+\frac{\hbar^2\pi}{m_{\perp}^*}n_S + \frac{q^2 n_S L}{4\epsilon_{\parallel}}+E_D . \tag{11}$$

This equation yields the maximum value of L compatible with a full depletion of the ϵ region, and consequently N_D^{ϵ} and V_0, for a given n_S. The calculated V_0 for different values of n_S are shown in Table V. From these results, we can conclude that an electron concentrated of the order of 10^{12} cm^{-2} leads to unrealistically high values of V_0 and N_D^{ϵ}.

Kress-Rogers *et al.*[19] have reported SdH results in which several series of oscillations are observed in each sample. That was interpreted by assuming the occupation of several electric subbands in an accumulation layer, and 2D electron concentrations as high as 10^{12} cm^{-2} were deduced. On the other hand, one can assume that several accumulation layers contribute to SdH spectrum in each sample and that only the lowest subband is occupied in each one. Then the highest fundamental field (21 T), with the Landau levels largely spin split as the authors discuss, leads to a maximum electron density of 5×10^{11} cm^{-2}.

It is obvious that if all 2D electrons were supplied by shallow donors in the ϵ layers, its concentration would not increase when the temperature is raised. At high temperatures some 2D electrons would be excited to the 3D conduction band, leaving an uncompensated charge in the planar defect. That would be screened by 3D electrons and a classical accumulation layer with an extension of the order of the Debye length would appear as a transition region between the 2D subbands and the neutral bulk region.

Nevertheless, the value of μ_H in low-tin-content samples at room temperature ($\mu_H<0.5\mu_3$ in several samples) indicates, through Eq. (4), that the 2D electron concentration n_2 can be even an order of magnitude higher than n_3. The annealing of those samples at 300 °C results in an increase of μ_H by a factor of 20 or more. Infrared absorption measurements clearly show a proportional increase in the intensity of the $1s$-$2p_{\pm}$ electronic transition,[62] revealing that the annealing process really creates

TABLE V. Parameters of 2D subbands in InSe in the size-quantization model: (1) areal electron concentration (2) localization parameter of the variational wave function, (3) Fermi level with respect to the bottom of the lowest subband, (4) energy of the lowest subband measured from the bottom of the well, (5) built-in potential, (6) shift of the energy levels in the thin ϵ layer due to size quantization, (7) maximum thickness of the fully depleted thin ϵ layer, (8) impurity concentration in the ϵ layer.

1 n_S (cm^{-3})	2 b_0 (10^6 cm^{-1})	3 E_F-E_0 (meV)	4 E_0 (meV)	5 E_B (meV)	6 V_0 (meV)	7 L (nm)	8 N_D^{ϵ} (cm^{-3})
10^{10}	0.987	0.17	5.8	0.76	25.2	13.65	1.5×10^{16}
3×10^{10}	1.424	0.51	12.1	1.98	33.1	11.92	5.0×10^{16}
10^{11}	2.126	1.71	26.9	5.25	52.4	9.47	2.1×10^{17}
3×10^{11}	3.067	5.13	56.0	11.92	91.5	7.16	8.4×10^{17}
10^{12}	4.581	17.09	124.9	27.72	188.2	5.00	4.0×10^{18}

new shallow donors. After annealing, μ_H slowly relaxes to the previous value, then there must be a mechanism through which shallow donor become deep and vice versa. That behavior can be understood if we assume that native shallow donors are interstitial atoms in the perfect γ region, which tends to be segregated to the stacking faults where the disorder and the electric field make the related levels to become deep. That occurs during the relaxation process after annealing. Then the complete electronic structure of 2D defects in InSe must include a high concentration of bound states located in energy below the bottom of 2D subbands [Fig. 6(c)]. In the temperature range from 100 to 500 K electrons can be excited from these deep donors to the 2D subbands. The leaving interstitial charges increase the field at the interface, lowering the bottom of the 2D subbands. At temperatures of the order of 600 K, when most deep donors are ionized, the electric repulsion makes them diffuse and to be redistributed more homogeneously in the perfect γ region where they become shallow.

In the model of Fig. 6(c), the bottom of the first subband is given by Eq. (8), with one difference: 2D electrons must compensate the ionized shallow donors in the ϵ region and the ionized deep donors in the stacking fault. We can write the following neutrality equation:

$$n_S=N_D^{\epsilon}\frac{L}{2}+N_T^{+}=n_{S0}+N_T^{+} . \tag{12}$$

n_{S0} is the areal density of 2D electrons in a 2D subband and N_T^{+} is the areal density of ionized deep donors in the stacking fault. This equation can be used to calculate the 2D electron concentration at each temperature. The results depend on how the deep level energy moves as the potential well increases. It seems reasonable to assume that it moves with the bottom of the lowest subband. According to the calculation of Martin and Wallis[63] for bound states created by a charge at the interface of a Si/SiO_2 inversion layer, the binding energy increases with the electric field at the interface. In our case the electric field will change by an order of magnitude. Nevertheless, we will assume, for simplicity, the binding energy ΔE_T to be constant. Then we have

$$n_S=n_{S0}+\frac{N_T}{1+2\exp\left[\frac{E_F-E_0}{kT}\right]\exp\left[\frac{\Delta E_T}{kT}\right]} . \tag{13}$$

At finite temperature the Fermi level is given by[64]

$$E_F-E_0=kT\ln\left[\exp\left[\frac{\pi\hbar^2 n_s}{m_{\perp}^{*}kT}\right]-1\right] . \tag{14}$$

In regards to the value of N_T, it can be estimated if one assumes that most In atoms in the stacking faults diffuse to the bulk γ InSe after annealing. Then N_T/n_{S0} is given by the ratio between the room-temperature electron concentration after annealing and the low-temperature electron concentration before annealing, which yields $N_T/n_{S0}\approx 20-100$. Figure 7 shows the temperature dependence of n_s for $n_{s0}=10^{11}$ cm^{-2}, $N_T=10^{13}$ cm^{-2}, and for different values of ΔE_T. The room-temperature concentration turns out to be of the order of 10^{12} cm^{-2}

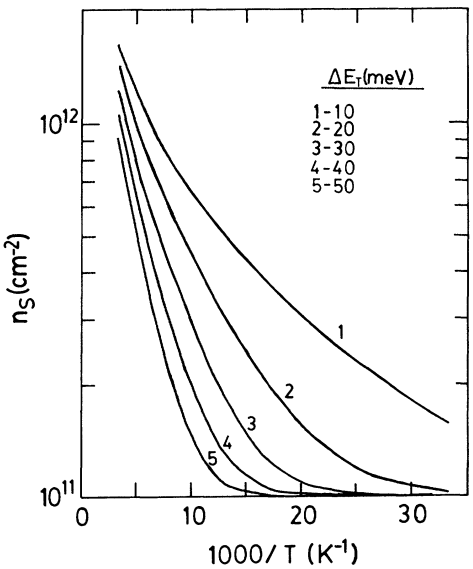

FIG. 7. Areal electron concentration vs the inverse temperature in a 2D subband for different values of the ionization energy of the deep donors adsorbed to the stacking fault.

for a large range of ΔE_T. For a mean distance between planar defects around 5 μm, it corresponds to an effective concentration of 10^{15} cm^{-3}. This is compatible with the experimental values of low-tin-content samples in which 2D electrons dominate. On the other hand, in the temperature range from 100 to 300 K the experimental electron concentration changes very slowly. In that sense, the lowest values of ΔE_T (10–20 meV) seems to be more plausible.

E. Homopolar optical-phonon scattering in the 2D subbands

The change of electron-scattering probabilities in a 2D system with respect to the 3D case has been widely discussed by several authors, especially for the 2D gas in AlGaAs/GaAs heterojunction.[65–68] In that which concerns phonon scattering, we should point out that a difference exists between polar (long-range interaction) and homopolar (short-range deformation-potential interaction) scattering. The 2D scattering probability of the second one, as we will see later, like all the deformation-potential mechanisms, is proportional to the localization parameter of the variational wave function,[65,66] which strongly lowers the 2D mobility with respect to the 3D value. This is not the case of polar scattering, for which 2D electron mobilities remain as high as in the 3D systems. That is the reason why very high mobilities can be attained in modulation doped GaAs heterostructures. Then we assume that in the InSe 2D accumulation layer the LO polar phonon limited electron mobility remains near the 3D value.

In order to obtain a first approximation to the electron 2D mobility limited by homopolar phonons we will assume that only the lowest subband is occupied and that only intrasubband scattering is present. The wave function of electron in the ground state is

$$\Psi_0 = Ce^{i\mathbf{k}_S\cdot\mathbf{r}_S}\left[\frac{2}{b_0^3}\right]^{1/2} z e^{-b_0 z/2} , \tag{15}$$

where $\mathbf{k}_S$ and $\mathbf{r}_S$ stand for the wave vector and position of electrons parallel to the plane defect. The perturbation Hamiltonian for homopolar optical scattering is[12]

$$V = D_0\left[\frac{\hbar}{2\rho V\omega}\right]^{1/2} e^{i\mathbf{q}\cdot\mathbf{r}}(a_{\mathbf{q}} + a^{\dagger}_{-\mathbf{q}}) . \tag{16}$$

D_0 is the deformation potential, ρ is the crystal density, V is the unit cell volume, ω is the phonon mode frequency, and q is the phonon wave vector; $a_{\mathbf{q}}$ and $a^{\dagger}_{-\mathbf{q}}$ stand for the annihilation and creation operators of phonon modes. The matrix elements of the transitions induced by the homopolar scattering are

$$|V_{\mathbf{k}_S\mathbf{k}'_S}|^{\pm} = D_0^2\frac{\hbar(N+\frac{1}{2}\pm\frac{1}{2})}{\rho V\omega}\frac{b_0^6}{(b_0^2+q_z^2)^3}\delta(\mathbf{k}_S-\mathbf{k}'_S\mp\mathbf{q}_S) , \tag{17}$$

where N is the phonon occupation number, $N=[\exp(\hbar\omega/KT)-1]^{-1}$, and the $\pm$ signs correspond to the emission or absorption of a phonon. The relaxation time will be

$$\begin{aligned}(\tau^{\pm}_{\mathbf{k}_S})^{-1} &= \frac{2\pi}{\hbar}\sum_{\mathbf{k}'_S\mathbf{q}}|V_{\mathbf{k}_S\mathbf{k}'_S}|^2\delta(E_{\mathbf{k}_S}-E_{k'_S}\mp\hbar\omega)\\ &= \frac{2\pi}{\hbar}\sum_{q}\frac{D_0^2\hbar^2(N+\frac{1}{2}\mp\frac{1}{2})}{2\rho V\omega}\frac{b_0^6}{(b_0^2+q_z^2)^3}\\ &\quad\times\delta(E_{\mathbf{k}_S}-E_{\mathbf{k}^{\pm}_S\mathbf{q}_S}\mp\hbar\omega) .\end{aligned} \tag{18}$$

The integral limits in q_z can be extended to infinity as the integrand quickly tends to zero for $q_z > b_0$. The integral on q_x and q_y has been calculated by Fivaz and Mooser.[11] We refer to Appendix I of Ref. 11 and obtain

$$\frac{1}{\tau_{2D}} = \frac{1}{\tau^{+}_{2D}} + \frac{1}{\tau^{-}_{2D}} , \tag{19}$$

$$(\tau^{+}_{2D})^{-1} = \begin{cases} 0, & E<\hbar\omega \\ 4\pi g^2_{\mathrm{var}}\omega(N+1), & E<\hbar\omega \end{cases}$$

(phonon emission) , (20)

$$(\tau^{-}_{2D})^{-1} = 4\pi g^2_{\mathrm{var}}\omega N \quad \text{(phonon absorption)} ,$$

where E is the electron kinetic energy for motion along the defect plane.

Following the above cited authors we can define an electron-phonon coupling constant

$$g^2_{\mathrm{var}} = \frac{D_0^2 m^*_{\perp}}{4\pi\rho V\omega^2\hbar^2}b_0\frac{3\pi}{8} = \frac{3\pi}{8}\left[\frac{\hbar^2 b_0^2}{2m^*_{\perp}\hbar\omega}\right]^{1/2} g^2 \tag{21}$$

in which the subscript "var" means that it has been obtained by using the variational wave function for 2D electrons and g^2 is the 3D electron-phonon coupling constant defined by Schmid.[12] It must be outlined that if intersubband scattering is taken into account, Eq. (21) is still valid, but the effective coupling constant is larger and depends on the localization parameter of the first excited subband.

Equation (21) is identical to that obtained by Fivaz and Mooser,[11] except in that which concerns the coupling constant. Nevertheless, it must be emphasized that the discussion of these authors on the value of the γ exponent as a function of the phonon energy is only valid for a nondegenerate 2D semiconductor. In our case, on the one hand, the coupling constant is temperature dependent, as n_S changes with temperature. On the other hand, the existence of the 2D electric subbands implies that most 2D states are below the Fermi level and then the Boltzmann statistics cannot be used. The 2D electron mobility must be calculated through

$$\mu_{2D} = \frac{q}{m^*_{\perp}}\langle\tau_{2D}\rangle = \frac{q}{m^*_{\perp}}\frac{\int_0^{\infty}E\tau_{2D}(E)\left[-\frac{\partial f_0}{\partial E}\right]dE}{\int_0^{\infty}E\left[-\frac{\partial f_0}{\partial E}\right]dE} , \tag{22}$$

where f_0 is the Fermi-Dirac distribution, in which

$E_F - E_0$ is calculated through Eq. (9). Figure 8 shows the temperature dependence of μ_2 between 30 and 300 K as calculated through Eqs. (19)–(22) for $\hbar\omega = 14.3$ meV (A_1' is the homopolar phonon) (Refs. 5 and 35) and for several values of n_{S0}, N_T, and ΔE_T. That calculation confirms our hypothesis of Sec. IV C regarding the lower value of μ_2 with respect to μ_3. On the other hand, results of Fig. 8 clearly illustrate the fact that the slope γ at 300 K is strongly dependent on ΔE_T.

Results of Fig. 8 also indicate that in the InSe 2D accumulation layers the homopolar phonons determine a quite low mobility, one order of magnitude lower than the polar phonon limited one, for areal concentrations of 2D electrons of the order of 10^{12} cm^{-2}, which would always be attained at room temperature (Fig. 7). Then, in this first approach to the problem we can neglect the effect of polar scattering for 2D electrons. We outline that it only refers to *high-temperature mobility.* Of course, at low temperature (1.5 K), electron mobility is not at all controlled by *any phonon mechanism,* but by ionized impurities in the ϵ layer or neutral impurities at the interface [Fig. 6(c)]. The conclusions of Howell *et al.*[20] about the scattering mechanisms that determine the CR linewidth cannot be extended to electron mobility. In a high-field CR experiment, 2D electrons are in well-defined Landau levels and are excited by ir photons with energies near the LO phonon energy. In a low-field HE experiment 2D electrons remain in thermal equilibrium with kinetic energies of the order of 1–2 meV.

Once μ_2 is calculated, μ_H can be obtained through Eq. (4), in which μ_3 is assumed to be controlled by polar and homopolar phonon scattering (Sec. IV A). It is obvious that the absolute value of μ_H and the slope γ will be determined by the ratio n_2/n_3. This model can also explain the large dispersion of the experimental results reflected in Table I, even if lattice scattering dominates.

In Fig. 9 we compare the experimental results for three samples from the 0.01%, 0.03%, and 0.1% doped ingots with the calculated value of μ_H. In that calculation we have taken $n_{S0} = 10^{11}$ cm^{-2}, $N_T = 2.5 \times 10^{12}$, and $\Delta E_T = 20$ meV. The bulk shallow donor concentration and the mean distance between planar defects d are adjusted so as to fit the room-temperature values of the electron mobility and electron concentration. They turn out to be 3.6×10^{14} cm^{-3}, 2.25 μm; 5.5×10^{14} cm^{-3}, 2.85 μm; and 2.25×10^{15} cm^{-3}, 1 μm for the 0.01%, 0.03%, and 0.1% Sn samples, respectively, which correspond to the expected increase of the 3D electron concentration with the tin content. The calculated mobility departs from the experimental values as temperature decreases due to the fact that impurity scattering has not been taken into account. Its influence will be discussed in another paper dealing with the transport properties of samples here studied at liquid-helium temperatures. It must be pointed out that the calculated μ_H is not very sensitive to the values of ΔE_T and N_T (in a reasonable range). Then the calculation of Fig. 9 should be considered as an example that illustrates how the model can reproduce the experimental results with reasonable values of the parameters. A complete quantitative interpretation is not possible

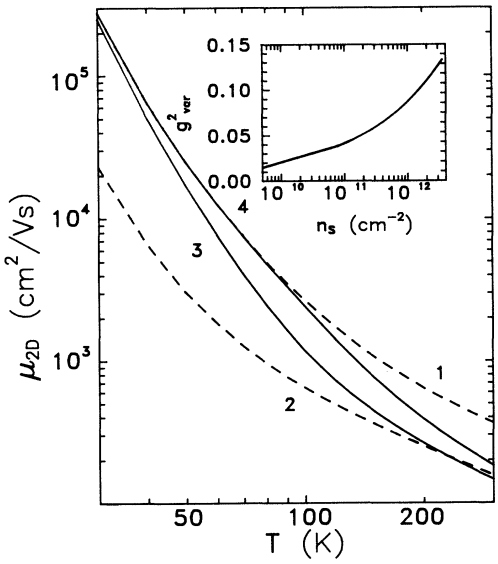

FIG. 8. Calculated 2D electron mobility vs absolute temperature in different conditions. Constant 2D electron concentration: 10^{11} (curve 1) and 10^{12} cm^{-2} (curve 2). Variable 2D electron concentration: $n_{S0} = 10^{11}$ cm^{-2}, $N_T = 5 \times 10^{12}$ cm^{-2}, $\Delta E_T = 10$ meV (curve 3), and $\Delta E_T = 50$ meV (curve 4). The inset shows the variation of 2D coupling constant with 2D electron concentration.

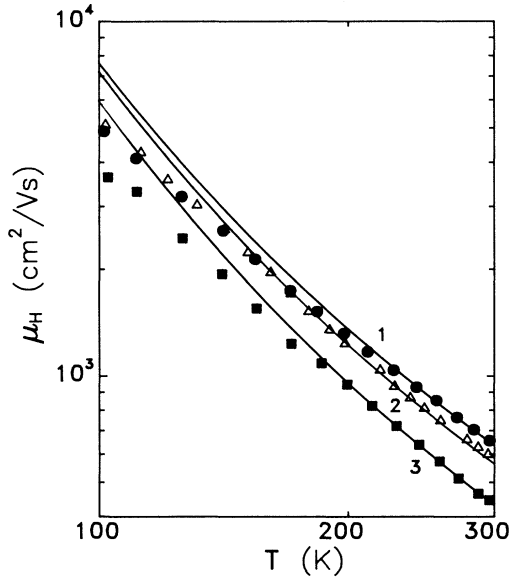

FIG. 9. Calculated electron Hall mobility vs absolute temperature for different values of the ratio of 3D to 2D electrons. The fixed parameters are $n_{S0} = 10^{11}$ cm^{-2}, $N_T = 2.5 \times 10^{12}$ cm^{-2}, and the fitting ones are $d = 1$ μm and $N_D = 2.25 \times 10^{15}$ cm^{-3} (curve 1), 2.85 and 5.5×10^{14} cm^{-3} (curve 2), 2.25 and 3.6×10^{14} cm^{-3} (curve 3), compared to experimental values for three samples from the 0.01% (■), 0.03% (△), and 0.1% (●) Sn-doped ingots.

without knowing the actual values of the parameters from the other kind of experiments.

V. CONCLUSIONS

HE measurements have been carried out in InSe samples doped with different amounts of Sn. The room-temperature electron Hall mobility exhibits an anomalous increase with electron concentration for low-tin-content samples. This effect has been shown to occur also when the electron concentration increases by photogeneration or thermal annealing. That can be interpreted by assuming that there are 3D and 2D electrons contributing to charge transport along the layers. The 3D electrons are created by excitation from shallow donors in the bulk γ-polytype regions of the sample. The 2D electrons are confined in electric subbands that are proposed to exist due to size-quantization effects in thin regions of the ϵ polytype located between two stacking faults. In the ϵ region electron states become higher than the conduction-band states in the γ polytype. Electrons are transferred to the γ region and the resulting electric field, together with the stacking fault potential barrier, confine them in 2D states. Localized deep levels are also proposed to exist in the stacking faults due to the adsorbed impurities. The 2D electron concentration increases with temperature due to excitation of electrons from those deep levels to the 2D subbands. More experimental studies on the shape of the potential along the c axis in InSe are needed in order to elucidate if this model is correct. High-resolution electron scanning microscopy and electron tunneling microscopy on good surfaces parallel to the c axis would supply very useful information.

It has been shown that the LO polar phonons are relevant in the scattering of 3D electrons, and the 3D mobility has been calculated through the iteration method. The introduction of polar scattering results in a reduction of the coupling constant of electrons to homopolar phonons.

A model for homopolar phonon scattering of 2D electrons has been proposed and the relaxation time was calculated by describing the electron localization along the c axis with a usual variational wave function. The 2D electron mobility has been shown to be determined by a coupling constant proportional to the variational localization parameter and to have a much lower value with respect to the 3D electron mobility for the same type of scattering. The temperature dependence of 2D electron mobility turns out to be strongly affected by the evolution of the 2D electron concentration. The Hall mobility has been calculated through a two-carrier model, showing that its absolute value and temperature-dependent slope can vary, within a quite large range, depending on the ratio between both types of carriers. This can be considered as the main conclusion of this work as it provides an explanation to the large dispersion of experimental results found in the literature. That dispersion turns out to be possible even when lattice scattering dominates.

ACKNOWLEDGMENTS

This work was supported through Spanish Government Comision Interministerial de Ciencia y Tecnologia Grant No. PPA86-0294. Thanks are due to Dr. A. Cantarero for his valuable help in the elaboration of computer programs and for a critical reading of the manuscript.

[1]S. M. Atakishiev and G. A. Akhundov, Phys. Status Solidi **32**, K33 (1969).

[2]Ph. Houdy, Thèse de troisième cycle, Université de Paris VII, 1982.

[3]Ph. Houdy, J. L. Maurice, J. M. Besson, J. Y. Laval, A. Chevy, and O. Gorochov, J. Appl. Phys. **61**, 5267 (1987).

[4]C. de Blasi, G. Micocci, A. Rizzo, and A. Tepore, Phys. Rev. B **27**, 2429 (1983).

[5]A. Segura, F. Pomer, A. Cantarero, W. Krause, and A. Chevy, Phys. Rev. B **29**, 5708 (1984).

[6]R. Cingolani, L. Vasanelli, and A. Rizzo, Nuovo Cimento D **6**, 383 (1985).

[7]S. Shigetomi, T. Ikari, Y. Koga, and S. Shigetomi, Jpn. J. Appl. Phys. **20**, L343 (1981).

[8]S. Shigetomi, T. Ikari, Y. Koga, and S. Shigetomi, Phys. Status Solidi A **86**, K69 (1984).

[9]R. Triboulet, C. Levy-Clemant, B. Theys, and A. Chevy, J. Cryst. Growth **79**, 984 (1986).

[10]V. K. Lukyanyuk, M. V. Tovarnitskii, and Z. D. Kovalyuk, Phys. Status Solidi A **104**, K41 (1987).

[11]R. Fivaz and E. Mooser, Phys. Rev. **163**, 743 (1967).

[12]Ph. Schmid, Nuovo Cimento B **21**, 258 (1974).

[13]R. Fivaz and Ph. Schmid, in *Optical and Electrical Properties*, edited by P. A. Lee (Reidel, Dordrecht, 1976).

[14]A. Bourdon, A. Chevy, and J. M. Besson, *Proceedings of the Fourteenth International Conference of Physics of Semiconductors* [Inst. Phys. Conf. Ser. **43**, 1371 (1979)].

[15]E. Kress-Rogers, R. J. Nicholas, J. C. Portal, and A. Chevy, Solid State Commun. **44**, 379 (1982).

[16]J. C. Portal, R. J. Nicholas, E. Kress-Rogers, A. Chevy, J. M. Besson, J. Galibert, and D. Perrier, *Proceedings of the Fifteenth International Conference of Physics of Semiconductors* [J. Phys. Soc. Jpn. Suppl. A **49**, 879 (1980)].

[17]R. J. Nicholas, E. Kress-Rogers, J. C. Portal, J. Galibert, and A. Chevy, Surf. Sci. **113**, 339 (1982).

[18]E. Kress-Rogers, G. F. Hoppert, R. J. Nicholas, W. Hayes, J. C. Portal, and A. Chevy, J. Phys. C **16**, 4285 (1983).

[19]E. Kress-Rogers, R. J. Nicholas, and A. Chevy, J. Phys. C **16**, 2439 (1983).

[20]D. F. Howell, R. J. Nicholas, C. J. G. M. Langerak, J. Singleton, T. J. B. M. Janssen, and A. Chevy, J. Phys. Condens. Matter **1**, 7493 (1989).

[21]A. Segura, K. Wünstel, and A. Chevy, Appl. Phys. A **31**, 139 (1983).

[22]B. Marí, A. Segura, and A. Chevy, Appl. Phys. A **45**, 579 (1988).

[23]A. Chevy, J. Cryst. Growth **67**, 119 (1984).

[24]A. Chevy, J. Appl. Phys. **56**, 978 (1984).

[25]H. Brooks, *Advances in Electronics and Electron Physics* (Academic, New York, 1955), Vol. 7, p. 85.

[26]C. Erginsoy, Phys. Rev. **79**, 1013 (1950).

[27]N. G. Aliev, I. G. Kerimov, and M. M. Kurbanov, Fiz. Tverd. Tela (Leningrad) **12**, 3707 (1973) [Sov. Phys.—Solid State **14**, 3106 (1973)].

[28]A. Segura, Thèse 3eme cicle, Université de Paris VI, 1977.
[29]N. Kuroda, O. Ueno, and Y. Nishina, J. Phys. Soc. Jpn. **55**, 581 (1986).
[30]M. Gauthier, A. Polian, J. M. Besson, and A. Chevy, Phys. Rev. B **40**, 3837 (1989).
[31]M. Schlüter, Nuovo Cimento B **13**, 313 (1973).
[32]U. Ya. Altshul and V. K. Bashenov, Phys. Status Solidi B **98**, K5 (1980).
[33]J. Bardeen and W. Shockley, Phys. Rev. **80**, 72 (1950).
[34]H. Fröhlich, Adv. Phys. **3**, 325 (1954).
[35]N. M. Gasalny, B. M. Yavadov, V. I. Tugirov, and E. A. Vinogradov, Phys. Status Solidi B **89**, K43 (1978).
[36]N. Kuroda and Y. Nishina, Solid State Commun. **34**, 481 (1980).
[37]N. Piccioli, R. Le Toullec, F. Bertrand, and J. C. Chervin, J. Phys. (Paris) **42**, 1129 (1981).
[38]I. G. Lang and U. S. Pashabekova, Fiz. Tverd. Tela (Lengingrad) **6**, 3640 (1965) [Sov. Phys.—Solid State **6**, 2913 (1965)].
[39]D. L. Rode, Phys. Rev. B **2**, 1012 (1970).
[40]B. R. Nag, *Electron Transport in Compound Semiconductors*, Springer Series in Solid State Sciences Vol. 11 (Springer, Berlin, 1980).
[41]B. Marí, A. Segura, and A. Chevy, Phys. Status Solidi B **130**, 793 (1985).
[42]F. Pomer, X. Bonet, A. Segura, and A. Chevy, Phys. Status Solidi B **145**, 261 (1988).
[43]P. Kirèev, *La Physique des Semiconducteurs* (Mir, Moscow, 1975).
[44]S. Sas, S. Muto, K. Kondo, H. Ishikawa, and S. Hiyamizu, Jpn. J. Appl. Phys. **24**, L602 (1985).
[45]A. Zrenner, Ph.D thesis, Technical University of München, 1987.
[46]A. Zrenner, F. Koch, and K. Ploog, Surf. Sci. **196**, 671 (1988).
[47]G. Gillman, P. Bois, E. Barbier, B. Vinter, D. Lavielle, M. Stohr, S. Najda, A. Briggs, and J. C. Portal, Semicond. Sci. Technol. **3**, 620 (1988).
[48]E. F. Schubert, B. Ullrich, T. D. Harris, and J. E. Cunnigham, Phys. Rev. B **38**, 8305 (1988).
[49]F. Bassani, G. Iadonisi, and B. Preziosi, Rep. Prog. Phys. **37**, 1099 (1974).
[50]G. L. Belenkii, M. O. Godzaev, and V. N. Zverev, Pis'ma Zh. Eksp. Teor. Fiz. **43**, 594 (1986) [JETP Lett. **43**, 769 (1986)].
[51]N. B. Brandt, V. A. Kulbachinskii, Z. D. Kovalyuk, and G. V. Lashkarev, Fiz. Tekh. Poluprovodn. **21**, 1001 (1987) [Sov. Phys.—Semicond. **21**, 613 (1987)].
[52]C. de Blasi, D. Manno, S. Mongelli, and A. Rizzo, Nuovo Cimento C **7**, 795 (1986).
[53]N. Kuroda and Y. Nishina, Solid State Commun. **28**, 439 (1978).
[54]L. N. Alieva, G. L. Belenkii, I. I. Reshina, E. Yu. Salaev, and A. S. Yakimova, Fiz. Tverd. Tela (Leningrad) **21**, 155 (1979) [Sov. Phys.—Solid State **21**, 90 (1979)].
[55]E. Aulich, J. L. Brebner, and E. Mooser, Phys. Status Solidi **31**, 129 (1969).
[56]S. Nagel, A. Baldereschi, and K. Maschke, J. Phys. C **12**, 1625 (1979).
[57]Yu. P. Guatenko, Yu. I. Zhirko, Z. D. Kovalyuk, and V. M. Kaminishkii, Fiz. Tverd. Tela (Leningrad) **28**, 3591 (1986) [Sov. Phys.—Solid State **28**, 2024 (1986)].
[58]Ph. Schmid, Ph.D. thesis, Ecole Politechnique Federal de Lausanne, Lausanne, 1974.
[59]K. Maschke and Ph. Schmid, Phys. Rev. B **12**, 4312 (1975).
[60]K. Maschke and H. Overhof, Phys. Rev. B **15**, 2058 (1977).
[61]F. F. Fang and W. E. Howard, Phys. Rev. Lett. **16**, 797 (1966).
[62]J. Martinez-Pastor (unpublished).
[63]B. G. Martin and R. F. Wallis, Phys. Rev. B **18**, 5644 (1978).
[64]F. Stern and W. E. Howard, Phys. Rev. **163**, 816 (1967).
[65]P. J. Price, Ann. Phys. (N.Y.) **133**, 217 (1981).
[66]P. J. Price, Surf. Sci. **113**, 199 (1982).
[67]K. Lee, M. S. Shur, T. J. Drummond, and H. Morkoç, J. Appl. Phys. **54**, 6432 (1984).
[68]W. Walukiewicz, H. E. Ruda, J. Lagowski, and H. C. Gatos, Phys. Rev. B **30**, 4571 (1984).